Analyst

Accepted Manuscript

This article can be cited before page numbers have been issued, to do this please use: F. X. Wang, C. Ye, S. Mo, L. L. Liao, X. F. Zhang, Y. Ling, L. Lu, H. Q. Luo and N. Li, *Analyst*, 2018, DOI: 10.1039/C8AN00895G.

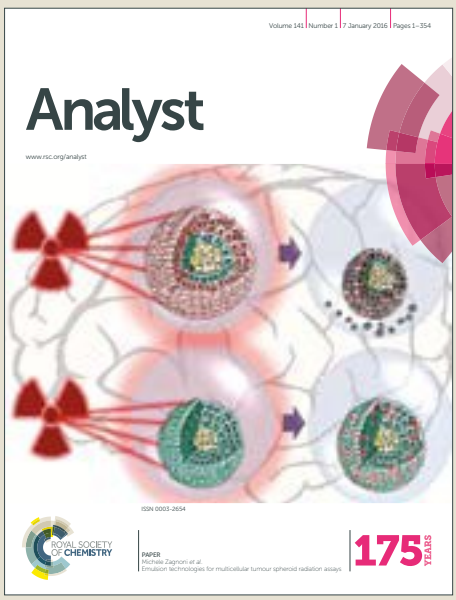

ROYAL SOCIETY OF CHEMISTRY

rsc.li/analyst

View Article Online
DOI: 10.1039/C8AN00895G

Analyst

ARTICLE

A novel "signal-on" photoelectrochemical sensing for ultrasensitive detection of alkaline phosphatase activity based on TiO_2/g-C_3N_4 heterojunction

Received 00th May 20xx,
Accepted 00th May 20xx

DOI: 10.1039/x0xx00000x

www.rsc.org/

Feng Xia Wang, Cui Ye, Shi Mo, Liu Li Liao, Xiao Fang Zhang, Yu Ling, Lu Lu, Hong Qun Luo* and Nian Bing Li*

Alkaline phosphatase (ALP) playing as a biomarker in some diseases including hepatitis, obstructive jaundice, osteoblastic bone cancer, and osteomalacia is important in clinical diagnosis. Furthermore, ALP activity detection is an essential hot topic in environmental monitoring, biomedical research, and other research field. Herein, a novel "signal-on" photoelectrochemical (PEC) biosensor based on ALP-catalyzed phosphorylation reaction was designed to sensitively detect ALP activity. In this design, the electron donor ascorbic acid was catalytically produced by ALP from L-ascorbic acid 2-phosphate trisodium salt *in situ*, which results in an increased photocurrent response signal. For immobilizing the ALP on the electrode surface, poly diallyl dimethyl ammonium chloride was used for the conjugation of ALP and photoactive material titanium dioxide (TiO_2) and graphite-like carbon nitride (g-C_3N_4) nanocomposites were prepared and characterized. The TiO_2 attached on g-C_3N_4 plays an important role for biosensing purpose due to their good biocompatibility and chemical/thermal stability while g-C_3N_4 provides the PEC response signal. Furthermore, the prepared TiO_2/g-C_3N_4 nanocomposites can effectively suppress the electron-hole recombination, improve the excitation conversion efficiency and make best use of the solar energy. The PEC biosensor for ALP activity detection displays a detection limit of 0.03 U/L (S/N = 3), which offers a new route for the ALP activity assay in human serum samples.

Introduction

Photoelectrochemical (PEC) biosensor represents a new emerging technology, which offers an innovative route for detecting various chemicals and has become more and more popular in recent decades.[1,2] Inspiringly, since the photoelectric effect was discovered by Edmond Becquerel in 1839,[3] the integration of PEC process with biosensor has became an innovative field. The PEC biosensor possesses anticipated potential in biological field compared to traditional electrochemical and optical methods owing to its merits of cheap instrument,[4-6] straightforward operation, high sensitivity, and low background signals.[7-10] Moreover, in order to obtain the highly efficient photon-to-electron conversion, the electron donor and acceptor existence and production *in situ* is essential for the construction of sensors and signal amplification.[11]

The polymeric graphitic carbon nitride material (g-C_3N_4) has emerged as a new class of photocatalyst owing to its high stability and visible-light driven band gap. As a metal-free and inorganic polymeric semiconductor material, g-C_3N_4 has a typical graphite-like layer structure and a strong covalent bonding within adjacent C-N layers[12]. Furthermore, the p-conjugated graphitic planes due to its sp^2 hybridization confer g-C_3N_4 a narrow band gap of 2.7 eV. Compared to the common wide band gap semiconductor photocatalysts such as $BiPO_4$, TiO_2, and ZnO, the highest occupied molecular orbital (HOMO) of the g-C_3N_4 is more negative, which makes this material tend to form heterojunctions with the wide band gap semiconductors, extending their visible light response.[13,14] Due to the high activity, superior-chemical stability, non-toxicity, large surface area, commercial availability, and other excellent advantages,[15] titanium dioxide (TiO_2) has been widely used in UV shielding,[16] photocatalysis,[17,18] paints, and solar cells,[19] and also played an important role in helping to ease the environmental and energy crisis through effective utilization of solar energy derived from photocatalysis and water photovoltaics.[20-22] Among these topics, photocatalysis is a promising research area for the semiconductive property of TiO_2. However, due to the wide band gap (3.0-3.2 eV), bare TiO_2 can only be excited by UV light at wavelengths less than 387.5 nm.[23]

Unfortunately, under 400 nm, UV light only accounts for 3-5% in sunlight,[24,25] which leads to a low conversion efficiency for the solar energy. In order to solve this problem, great efforts have been devoted to modify bare TiO_2 with narrow band gap or organic semiconductive materials during the past decades.[26] Moreover, for biosensor, the fabricated TiO_2/g-C_3N_4/GCE electrodes were activated by casting 5 μL of 2 % poly diallyl dimethyl ammonium

Key Laboratory of Eco-Environments in Three Gorges Reservoir Region (Ministry of Education), School of Chemistry and Chemical Engineering, Southwest University, Chongqing 400715, PR China. Corresponding Author. E-mail address: luohq@swu.edu.cn (HQ Luo);linb@swu.edu.cn (NB Li).
†Electronic Supplementary Information (ESI) available: Fig. S1 and Table S1-S2. See DOI: 10.1039/x0xx00000x

View Article Online
DOI: 10.1039/C8AN00895G

chloride containing 0.5 M NaCl for 30 min. The proteins can be immobilized on the TiO_2-based semiconductor nanostructures due to their high biocompatibility and good chemical/thermal stability.[27-29] What is more, the enzymatic hydrolysis process generates the product, ascorbic acid (AA), containing enediol-ligand, which has a large affinity for Ti atoms on TiO_2 nanosheets.[30-33] The electrochemical properties of TiO_2-based devices are influenced not only by the textural properties of the TiO_2, but also by the crystalline form of the TiO_2. Not only the adequate pore distributions, but also a high surface area are especially beneficial to the fabrication of TiO_2 based bioelectronic devices, because these properties provide high accessibility for the target analyte to the device surface as well improve the interaction between TiO_2 and biomolecules. Therefore, it is necessary to find a material to improve the photocatalytic property of TiO_2. To the best of our knowledge, combining g-C_3N_4 with TiO_2 can exhibit a high photoelectrochemical biosensing property. As expected, after TiO_2 was attached on g-C_3N_4, the photo-generated electrons produced from g-C_3N_4 can migrate to the conduction band (CB) of TiO_2 through the interface between g-C_3N_4 and TiO_2. Due to the more positive valence band (VB) edge of the TiO_2, the holes generated by visible light cannot be transferred to the VB of TiO_2, which leads to the migration of the electrons to TiO_2 and the holes stay in the g-C_3N_4.[34] This electron hole transfer mechanism can accelerate the spatial charge separation and effectively suppress the electron-hole pair recombination in the designed TiO_2/g-C_3N_4 nanocomposites.

In this paper, we synthesized TiO_2/g-C_3N_4 nanocomposites by a hydrothermal method and the nanocomposites exhibit an enhanced PEC performance due to the unique electronic band structure between g-C_3N_4 and TiO_2, which indicates that the recombination of photo-induced electro-hole pairs is suppressed, thus improving the PEC performance. In addition, using this nanocomposites, alkaline phosphatase (ALP) can be fixed to a glassy carbon electrode surface *via* poly diallyl dimethyl ammonium chloride and catalytically hydrolyze L-ascorbic acid 2-phosphate trisodium salt (AAP) to generate electron donor AA *in situ*, resulting in an enhanced photocurrent and improving the PEC performance for target ALP detection. Furthermore, As a proof-of-concept, the resultant TiO_2/g-C_3N_4/GCE was applied as a photoelectrode material to construct a fresh PEC sensing for ALP assay upon ALP-based amplification strategy and *in situ* generation of electron donors *via* an enzymatic-reaction. When AA was produced *in situ*, it can capture the holes in the VB of TiO_2. Such a synergy effect in the designed protocol can accelerate the spatial charge separation and suppress the electron-hole recombination, and hence increase the PEC performance for ALP assay. The TiO_2/g-C_3N_4 based fabrication process of the PEC biosensor and the assay principle of PEC response for target ALP is schematically illustrated in Scheme 1. However, in the traditional PEC biosensing systems, electron donors or acceptors are directly added to the electrolytic cell, which are not conducive to the development of living cell biosensor systems because of the lacking of electron donors or acceptors in living cells or organisms.[23,35-37] Furthermore, we built a simple operated PEC biosensor using simple equipment, which is easy to implement, consumes less sample, and has a good repeatability and high recovery ratio. With the integration of the nanocomposites of

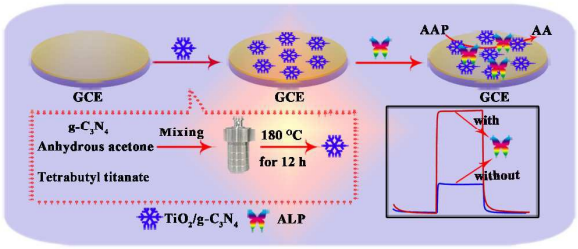

Scheme 1. Schematic illustration of the fabrication processes of the PEC biosensor and the assay principle of PEC response.

TiO_2/g-C_3N_4 and ALP, the constructed ALP-based amplification strategy can generate the electron donor *in situ*. Thus, the PEC biosensor for ALP activity detection exhibits a signal-on photocurrent response. Specially, the purpose of this study is to design an innovative photoelectrode material and *in situ* produce electron donors via the enzymatic hydrolysis reaction, introducing a method for constructing the highly efficient signal-on PEC biosensor.

Experimental section

Materials and reagents

ALP was purchased from Sangon Biotech Co., Ltd. (Shanghai, China). L-Ascorbic acid 2-phosphate trisodium salt, poly diallyl dimethyl ammonium chloride, and 2-amino-2-(hydroxymethyl)-1,3-propanediol (Tris) were purchased from Sigma-Aldrich (St. Louis, MO). Ferrocyanide/ferricyanide solution ($Fe(CN)_6^{3-/4-}$, 5 mM) was prepared by dissolving potassium ferricyanide and potassium ferrocyanide in 0.1 M phosphate buffer (0.1 M KCl, 0.1 M KH_2PO_4, 0.1 M Na_2HPO_4, pH 7.4). Human blood serum was obtained from the hospital of southwestern university (Chongqing, China). Other chemicals were of analytical reagent grade and used as received. The buffer solutions, 0.1 M Tris-HCl (pH 7.0, 7.5, 8.0, 8.5, 9.0, 9.5), were prepared by adding 1.2114 g of Tris to 100 mL of ultrapure water and being regulated with different concentrations of hydrochloric acid. Various concentrations of AAP were obtained by dissolving certain amount of AAP into the Tris-HCl (0.1 M, pH 8.2) buffer. ALP with various concentrations were obtained by diluting ALP with the Tris-HCl (0.01 M, pH 8.2) buffer containing 5 mM $MgCl_2$ and 0.1 mM $ZnCl_2$. Ultrapure water (18.2 MΩ cm) was used throughout the experiments.

Characterizations

The field-emission scanning electron microscopy (FESEM) images were recorded on a JEOL-7800F scanning electron microscopy (INCA X-Max 250, Japan Electron Optics Laboratory Co., Japan). The X-ray photoelectron spectroscopy (XPS) analysis was recorded on a Thermo ESCALAB 250Xi spectrometer (Thermoelectricity Instruments, USA) with the light source of Al Ka X-ray (1486.6 eV). Fourier transform infrared (FT-IR) spectra were taken with a Bruker IFS 113v spectrometer (Bruker, Germany). The X-ray diffraction (XRD) pattern was investigated on an XRD-7000 (Shimadzu, Japan) with Cu Kα source radiation at the range of 10° - 70° with a scanning rate of 2° min^{-1}. The transmission electron microscopy (TEM) image was obtained using a JEM-2100 (TEM, JEOL-2100, Japan) equipped

View Article Online
DOI: 10.1039/C8AN00895G

with a field emission gun (FEG) at 200 kV. Electrochemical measurements were carried out on a CHI 660B electrochemical workstation (Shanghai Chenhua Instruments Co., China) and the PEC measurements were recorded on a PEAC 200A (Tianjin AiDa Hengsheng Technology Co., Ltd., China) with a conventional three-electrode cell at room temperature, where the platinum wire worked as a counter electrode, the modified glassy carbon electrode (GCE, Φ = 3 mm) used as a working electrode, and the Ag/AgCl electrode worked as the reference electrode.

Synthesis of TiO_2/g-C_3N_4 nanocomposites

The g-C_3N_4 nanoflake was synthesized according to a previously reported procedure by the polymerization of melamine at a high temperature[38]. In detail, the alumina crucible containing 4.0 g of melamine was heated to 550 °C with the heating rate of 2 °C/min and maintained at this temperature for 2 h. In addition, another two hours were hold at this temperature in order to deammoniation. While TiO_2 nanosheets were prepared by adding 1.2 mL of hydrofluoric acid carefully to 10 mL of tetrabutyl titanate and then the mixture was transferred into a Teflon-lined stainless steel autoclave. The container was maintained at 180 °C for 24 h and the white product was centrifuged at 10000 rpm for 15 min and washed with acetone and ultrapure water for three times successively. Finally, the white product was dried at 60 °C for 8 h. The TiO_2/g-C_3N_4 nanocomposites were synthesized using the solvothermal method according to the literature[39] with proper modifications. Typically, 0.2415 g of g-C_3N_4 yellow powder was homogeneously dispersed in 15 mL of acetone by ultrasonication for 30 min. Subsequently, 0.5 mL of tetrabutyl titanate was added dropwise to the above solution under vigorous stirring. The mixed suspension was allowed to stir for 30 min at room temperature. Finally, the achieved suspension was transferred into a Teflon-lined stainless steel autoclave and maintained at 180 °C for 12 h. The product was centrifuged at 10000 rpm for 15 min and washed with acetone and ultrapure water for three times successively, and dried at 60 °C.

Preparation of electrodes

A glassy carbon electrode (GCE, Φ = 3 mm) was polished on chamois leather with alumina powder (0.5 and 0.05 μm), rinsed thoroughly with ultrapure water, cleaned ultrasonically in ethanol and ultrapure water, and dried with nitrogen. After that, TiO_2/g-C_3N_4 nanocomposites (10 μL, 3 mg/mL) was dropped onto the surface of the well-polished GCE and dried in the air. The ultrapure water was used as the solvent in the prepared progress of the composites of 3 mg/mL TiO_2/g-C_3N_4, and after 20 min ultrasonic dispersion a uniform dispersive suspension was formed. The fabricated TiO_2/g-C_3N_4/GCE electrodes were then activated by casting 5 μL of 2 % poly diallyl dimethyl ammonium chloride containing 0.5 M NaCl for 30 min for the conjugation of ALP. Next, ALP (6 μL) with various concentrations was added on the electrode surface and then incubated for 6 h in the refrigerator at 4 °C. After the modification processes, the prepared electrode was washed with 0.01 M Tris-HCl buffer (pH 8.1) to remove excess reagents. The modified electrode was marked as the ALP/TiO_2/g-C_3N_4/GCE, which was stored in the refrigerator at 4 °C before electrochemical experiments.

PEC detections for alkaline phosphatase and data analysis

The PEC detections of ALP were performed at room temperature in a 4 mL cell. The prepared electrode of ALP/TiO_2/g-C_3N_4/GCE was incubated with 0.08 M AAP at 37 °C for 50 min. After that, the resulting modified electrode was rinsed with the Tris-HCl buffer and the photocurrent intensity of the ALP/TiO_2/g-C_3N_4/GCE was measured in the Tris-HCl buffer (0.1 M, 4 mL, pH 8.0), followed by a visible-light irradiation with an applied potential of 0.2 V.

Results and discussion

Characterization of materials

In this work, the TiO_2 attached on g-C_3N_4 is necessary to conjugate ALP and g-C_3N_4 providing PEC response signal. To observe the microscopic structure, the SEM images of TiO_2 nanosheets and g-C_3N_4 are exhibited in Fig. 1A and B, respectively. Clearly, the sheet structure can be observed for the prepared TiO_2. The g-C_3N_4 in Fig. 1B shows a typical morphology of aggregation, larger size and flaky structure. Fig. 1C shows the TEM and HRTEM (inset) images of TiO_2/g-C_3N_4 nanocomposites and confirms the clear lattice spacing of ~0.34 nm corresponding to the (101) lattice plane of anatase TiO_2, indicating that the surface of g-C_3N_4 was densely coated with TiO_2. Importantly, the prepared nanocomposites can suppress the recombination of photo-induced electro-hole pairs, which may be ascribed to the unique electronic band structure between TiO_2 and g-C_3N_4. This well matched band structure may also improve the PEC performance for subsequent ALP detection. The XRD patterns of the g-C_3N_4 (curve a), TiO_2 (curve b), and TiO_2/g-C_3N_4 (curve c) nanoflake are presented in Fig. 1D. As depicted in Fig. 1D (curve a), two characteristic peaks corresponding to (100) and (002) lattice planes, respectively, can be seen clearly in the sample of g-C_3N_4. Curve b shows that all the diffraction peaks can be perfectly indexed with major peaks related to (110), (101), (-112), (020), and (204) planes, the diffraction peaks of the TiO_2 phase can be observed at 2ϑ = 25.28° and 48.0° corresponding to the characteristic absorption band of anatase TiO_2 without impurity phase. The diffraction peak at 25.28° is attributed to the (101) crystal plane and no characteristic peaks of rutile phase TiO_2 appear in curve b (Fig. 1D). However, curve c (Fig. 1D) only shows the specific peaks of the anatase TiO_2 whereas the peaks of g-C_3N_4 are not observed or inconspicuous in the sample of TiO_2/g-C_3N_4, which is mainly due to the low content of g-C_3N_4 in the nanocomposites. In addition, the lower intensity and wider diffraction peaks of TiO_2/g-C_3N_4 signify the two-phase composition of TiO_2 and g-C_3N_4.[6,40]

In order to further confirm the successful synthesis of TiO_2/g-C_3N_4 nanocomposites, XPS was utilized for elemental analysis (Fig. 2A, B, C, D, and E). As shown in Fig. 2A, the characteristic peaks of C1s, N1s, O1s, and Ti2p regions are clearly observed in the full scanning range for TiO_2/g-C_3N_4 nanocomposites. The atomic percentage of TiO_2/g-C_3N_4 (Fig. 2G) obtained from the XPS measurement illustrates the quantitative composition of the elements. Fig. 2B displays the XPS peak of C1s (284.85 eV), which may result from the impurity carbon introduced in the sample. The XPS peak at 288.30 eV can be attributed to the carbon of sp^2 hybridization.[41,42] As seen in Fig. 2C, the peaks at 398.35, 399.20,

View Article Online
DOI: 10.1039/C8AN00895G

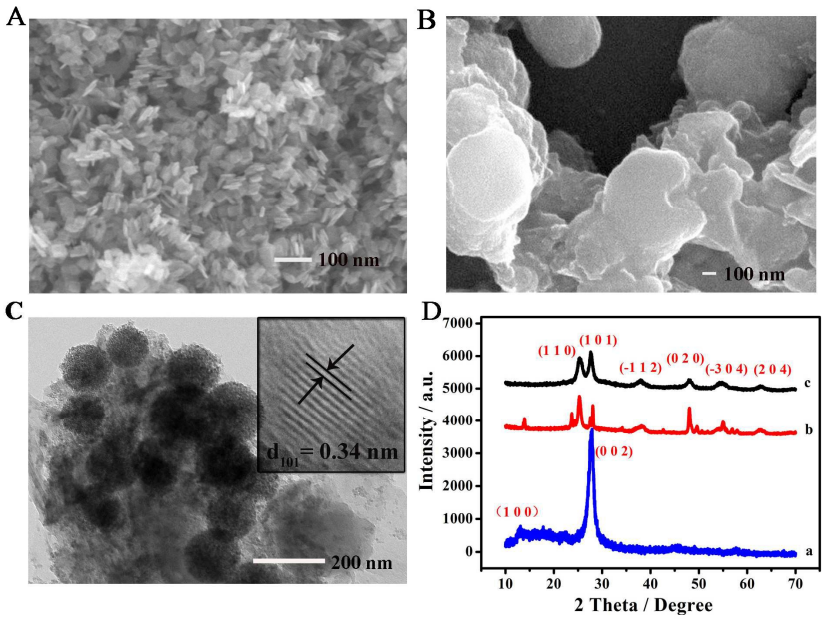

Fig. 1. FESEM images of (A) TiO_2 nanosheets and (B) g-C_3N_4. (C) TEM and HRTEM (inset) images of the TiO_2/g-C_3N_4 nanocomposites. (D) XRD patterns of the g-C_3N_4 (curve a), TiO_2 (curve b), and TiO_2/g-C_3N_4 (curve c)

and 400.20 eV correspond to the nitrogen of sp^2 hybridization (C=N-C), nitrogen produced by the polymerization of melamine (N-(C_3)), the peaks at 529.92, 458.60, and 464.40 eV in Fig. 2D and 2E can be assigned to O1s region, $Ti2p_{3/2}$, and $Ti2p_{1/2}$, respectively.[43,44] The peak around 472.00 eV in Fig. 2E proves the existence of the satellite peak of the TiO_2, which suggests the occurrence of a lower energy shake-up satellite due to charge transfer transition.[45,46] In conclusion, the XPS measurement indicates the successful preparation of TiO_2/g-C_3N_4 nanocomposites. Fig. 2F displays the Fourier transform infrared (FT-IR) characteristics of TiO_2, g-C_3N_4, and TiO_2/g-C_3N_4. For g-C_3N_4, the absorption bands located at 1239.59, 1319.19, and 1407.78 cm^{-1} are attributed to C–N stretching vibration of aromatic ring, while the absorption bands at 1638.08 and 807.84 cm^{-1} result from C-N stretching vibration and the out-of plane bending modes of C-N heterocycle, respectively.[47] Because of the stretching modes of N-H or NH_2 groups at the defect sites of the aromatic ring, a broad band can be observed at 3154.30 cm^{-1}. The strong absorption of the TiO_2/g-C_3N_4 and TiO_2 at approximately 891.45 cm^{-1} is due to the stretching vibration of the Ti-O-Ti bond, and the broad absorption peak at 3424.30 cm^{-1} is related to the stretching vibration of the surface active hydroxyl group of titania. Compared to the pure TiO_2, the FT-IR spectrum of TiO_2/g-C_3N_4 is very similar to that of g-C_3N_4, except for the stronger absorption band intensity. These phenomena confirm that the nanocomposites are formed between g-C_3N_4 and TiO_2.[48,49]

Photoelectrochemical property of TiO_2/g-C_3N_4 nanocomposites

The PEC properties of TiO_2, g-C_3N_4, and TiO_2/g-C_3N_4 nanocomposites were investigated by photocurrent technique and cyclic voltammograms (CV). Fig. 3A shows that the PEC photocurrent response of TiO_2/g-C_3N_4 nanocomposites modified electrode under the irradiation of visible-light in the period of 180-200 s is sharply enhanced (curve c) compared to that without the irradiation of visible-light in the period of 160-180 s, and is higher than that of g-C_3N_4 modified electrode (curve b) and TiO_2 modified electrode (curve a), suggesting that with the irradiation of visible-light, the TiO_2/g-C_3N_4 nanocomposites can efficiently enhance the photocurrent response owing to the well matched energy level structures between TiO_2 and g-C_3N_4. Under the irradiation of visible-light, the signal response increases rapidly and achieves a stabilized value for the fast excitation, separation, and transfer of photo-induced electrons in the TiO_2/g-C_3N_4 nanocomposites. The proposed photocurrent-transducer mechanism is shown in Scheme 2. Compared to TiO_2, g-C_3N_4 possesses more negative lowest unoccupied molecular orbital (LUMO) and HOMO potentials. Therefore, the photogenerated electrons of g-C_3N_4 can be migrated to the CB of TiO_2 through the interface between g-C_3N_4 and TiO_2. In addition, due to the more positive VB edge of the TiO_2, the holes generated by visible-light cannot be transferred to the TiO_2. As a result, the electrons are moved to TiO_2 and the holes keep in the g-C_3N_4. When the electron donor, AA, was produced *in situ*, it can capture the holes in the VB of TiO_2. Such a synergy effect in the designed protocol can accelerate the spatial charge separation and suppress the electron-hole recombination, and hence increase the PEC performance for subsequent assay. It has been reported that the electron-hole pairs at irradiation generated from the TiO_2/g-C_3N_4 nanocomposites are key to the generation of photocurrent response, which depends on the LUMO and the HOMO potentials.[6,50] For g-C_3N_4, the LUMO and HOMO potentials are 1.57 and -1.12 eV, respectively.[51-53] Also, the CB and VB of TiO_2 are -0.29 and 2.91 eV, respectively.[54,55] This effect improves the excitation and conversion efficiency. The recombination of photo-induced electro-hole pairs is suppressed for the well matched energy band between TiO_2 and g-C_3N_4, which is conducive to the improvement of

View Article Online
DOI: 10.1039/C8AN00895G

Analyst

ARTICLE

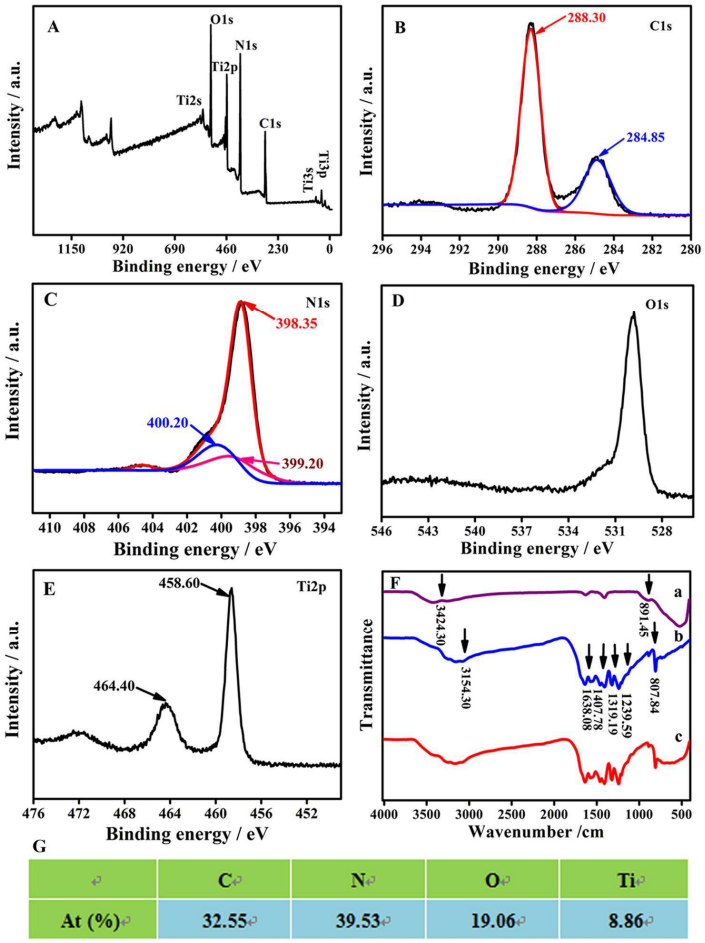

	C	N	O	Ti
At (%)	32.55	39.53	19.06	8.86

Fig. 2. XPS analysis of (A) the full region for TiO_2/g-C_3N_4 nanocomposite, (B) C1s region, (C) N1s region, (D) O1s region, and (E) Ti2p region. (F) FT-IR spectra of TiO_2 (a), g-C_3N_4 (b), and TiO_2/g-C_3N_4 (c). (G) The atomic percentage of TiO_2/g-C_3N_4 nanocomposite.

PEC performance for subsequent ALP detection[56,57]. In order to confirm the successful construction of each step of the electrode, the electrochemical characterization of the stepwise-modified electrode was executed by CV in a 5.0 mM $[Fe(CN)_6]^{3-/4-}$ solution. As represented in Fig. 3B, a couple of quasi-reversible redox peaks are achieved at the bare GCE (curve a), after being modified with the TiO_2/g-C_3N_4 nanocomposites on the bare GCE surface, an obvious decrease in redox peak current is achieved (curve b). When ALP is immobilized onto the electrode, an obviously decreased redox peak is observed due to its feature of obstructing the electron transfer (curve c). Followed by the introduction of AAP on the above electrode, the current is further decreased, which is attributed to the hindrance of the electron transfer (curve d).

Optimization of experimental conditions

Fig. S1A (see more details in supporting information) depicts the effect of pH on the response of PEC biosensor in a series of 0.1 M Tris-HCl buffer (pH = 7.0, 7.5, 8.0, 8.5, 9.0, 9.5). The commonly used supporting electrolyte for photocurrent measurements was phosphate buffer. However, the inorganic phosphate has an inhibitory effect on ALP. Thus, the Tris-HCl (0.1 M, pH 8.0) buffer was selected in this system. The photocurrent response increases with increasing pH value, and reaches to the maximum value at pH 8.0, because alkalescence environment can enhance the activity of ALP. However, when pH exceeds 8.0, the photocurrent decreases gradually. This is because ALP loses its activity under high alkaline condition. The results are consistent with those in the literature.[58,59]

View Article Online
DOI: 10.1039/C8AN00895G

Analyst

ARTICLE

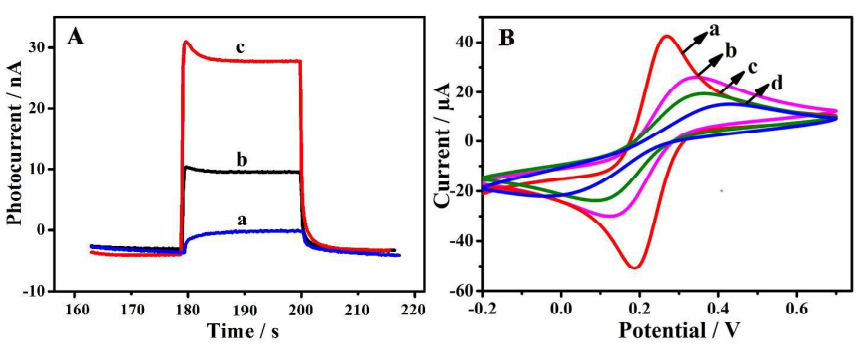

Fig. 3. (A) Photocurrent response of the prepared biosensor of (a) TiO_2/GCE, (b) g-C_3N_4/GCE, and (c) TiO_2/g-C_3N_4/GCE (B) CV profiles in 5.0 mM $[Fe(CN)_6]^{3-/4-}$ at a scan rate of 50 mV/s for the (a) bare GCE, (b) TiO_2/g-C_3N_4/GCE, (c) ALP/TiO_2/g-C_3N_4/GCE, and (d) AAP/ALP /TiO_2/g-C_3N_4/GCE.

Thus, pH 8.0 was chosen as the optimal pH value for the subsequent detections.

The influence of AAP concentration is exhibited in Fig. S1B. Increasing AAP concentration can improve the PEC photocurrent, and the photocurrent response reaches to the maximum value at the concentration of 0.08 M. When the concentration of AAP exceeds 0.08 M, as the concentration increases, the photocurrent reaches a stable value. Considering the photocurrent intensity and the consumption of the reagents, the optimum concentration of AAP used in this work is 0.08 M. The incubation time of ALP also plays an important role in the analytical performance.

In order to immobilize more ALP on the electrode surface, the incubation time was optimized. The photocurrent response of ALP/TiO_2/g-C_3N_4/GCE under different incubation time (4, 5, 6, 7, 8, and 9 h) was detected in the 0.1 M Tris-HCl buffer (pH = 8.0). As shown in Fig. S1C, the photocurrent increases with increasing incubation time and levels off after 6 h, illustrating an equilibrium state for this sensing system under this condition. Hence, 6 h is chosen as the optimized incubation time for immobilizing ALP in this study.

In the constructed PEC biosensor, TiO_2/g-C_3N_4 works not only as a signal probe, but also an immobilizer for ALP. Thus, the detection sensitivity and photocurrent intensity can be affected significantly by the concentration of TiO_2/g-C_3N_4. Fig. S1D shows the influence of TiO_2/g-C_3N_4 concentration on the PEC response. The photocurrent is improved gradually with the augment of TiO_2/g-C_3N_4 concentration at the range of 2.0 - 3.0 mg/mL, and reaches to the maximum value at 3.0 mg/mL. When the concentration of TiO_2/g-C_3N_4 exceeds 3.0 mg/mL, the photocurrent decreased gradually. The reason leading to this result may be because the thick film of TiO_2/g-C_3N_4 could improve the electron transfer resistance and decrease the photocurrent. Thus, 3.0 mg/mL TiO_2/g-C_3N_4 was selected as the optimal concentration.

The effect of reaction time between ALP and AAP was also studied in the AAP solution for 20, 30, 40, 50, 60, and 70 min, respectively. As shown in Fig. S1E, before the reaction time of 50 min, with increasing reaction time, the photocurrent is increased, when the reaction time exceeds 50 min, the photocurrent decreases. As a result, 50 min was selected as the optimal reaction time between ALP and AAP.

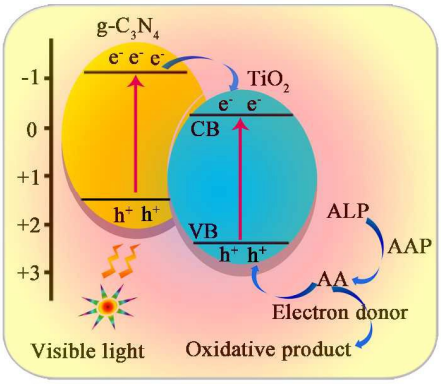

Scheme 2. The scheme for visible light-driven electron-hole excitation, separation and transfer mechanism of the TiO_2/g-C_3N_4 composite.

Calibration curve for ALP activity

The sensitivity of the prepared PEC biosensor for ALP activity detection was studied under optimized experimental conditions, and the relationship between ALP activity and PEC response is shown in Fig. 4A. The PEC photocurrent response increases with increasing ALP activity. After the incubation of ALP on the prepared TiO_2/g-C_3N_4/GCE electrode, AAP was added and hydrolysed to

View Article Online
DOI: 10.1039/C8AN00895G

Analyst

ARTICLE

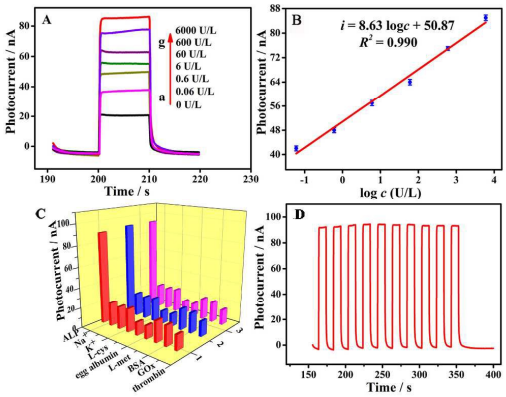

Fig. 4. (A) PEC responses of the prepared biosensor in 0.1 M pH 8.0 Tris-HCl buffer. ALP concentration: (a) 0 U/L, (b) 0.06 U/L, (c) 0.6 U/L, (d) 6 U/L, (e) 60 U/L, (f) 600 U/L, and (g) 6000 U/L. (B) the relevant calibration curve for ALP activity detection. (C) Selectivity of the PEC biosensor towards various targets: 15 nM thrombin, 15 nM GOx, 5 μg/mL BSA, 15 nM L-met, 15 nM egg albumin, 15 nM L- cys, 15 nM K^+ and 15 nM Na^+ in mixed solution. 1, 2 and 3 depict the serial number of three parallel measurements, respectively. (D) PEC photocurrent response of the fabricated biosensor after scanning for 10 cycles, the ALP concentration is 6000 U/L.

generate AA *in situ*, enhancing the PEC response. Fig. 4B displays a well linear relationship between the PEC intensity and the logarithm of the ALP activity with a linear equation of $i = 8.63 \log c_{ALP} + 50.86$ ($R^2 = 0.990$). The linear range for ALP activity is from 0.06 to 6000 U/L with a detection limit of 0.03 U/L, which is wider than that of the reported methods.[39,60,61] Additionally, we compare the analytical performance of the PEC biosensor with previously published studies and the results are shown in Table S1. Clearly, the prepared biosensor obtains a wider linear range and a lower detection limit in the experimentation of ALP activity detection.

Selectivity, repeatability and stability of the prepared biosensor

In order to evaluate the selectivity of the prepared PEC response biosensor, some similar enzymes and proteins, including 15 nM thrombin, 15 nM glucose oxidase (GOx), 5 μg/mL bovine serum albumin (BSA), 15 nM L-methionine (L-met), 15 nM egg albumin, 15 nM L-cys, 15 nM K^+, and 15 nM Na^+, were employed to replace ALP in the system on three independence modified electrodes. As depicted in Fig. 4C, the biosensor shows negligible PEC response to thrombin, GOx, BSA, L-met, egg albumin, L-cys, K^+, and Na^+, indicating that only the ALP can trigger the amplifying strategy and the designed system possesses good selectivity. The values of relative standard deviation (RSD) are usually utilized to clarify the repeatability of the prepared PEC biosensor. Under the same experimental conditions, the ALP/TiO_2/g-C_3N_4/GCE electrode shows good photocurrent repeatability after 10 cycles shown in Fig. 4D, indicating that the proposed biosensor was stable. For the measurements of intra-assay and inter-assay, the RSD of intra-assay is less than 5.0 % while the RSD of inter-assay for five modified electrodes is 6.8 %. The PEC response signal for the prepared electrodes reduces by 11.2 % after kept in the refrigerator at 4 °C for two weeks. This phenomenon indicates an excellent stored stability of the composite material and an acceptable repeatability of the designed PEC biosensor.

Real sample analysis

To evaluate the application potential and the analytical reliability of the designed PEC biosensor, the ALP concentrations in human serums were tested and the experiments of recovery were performed by assay of ALP-spiked human serums. We prepared a series of samples by adding various concentrations of ALP to human blood serum. As shown in Table S2, the recoveries range from 93.3 % to 103.7 % and the RSDs range from 4.6 % to 6.3 %, demonstrating the good practicability of the designed PEC biosensor for ALP activity detection in real biological samples.

Conclusion

In summary, we successfully developed a PEC biosensor for the detection of ALP activity based on the hydrolytic reaction of ALP and TiO_2/g-C_3N_4 nanocomposites. Efficient electron transfer processes in designed TiO_2/g-C_3N_4 nanocomposites can effectively suppress the electron-hole recombination and improve the excitation and conversion efficiencies. Simultaneously, the large accessible surface area for the immobilization of ALP is provided by the attachment of TiO_2 on g-C_3N_4. The well prepared PEC biosensor presents an outstanding performance with the detection limit of 0.03 U/L for ALP activity and a wide linear range of 0.06-6000 U/L. Such a sensitive and simple design can be developed as a general basis for probing other targets.

View Article Online
DOI: 10.1039/C8AN00895G

Acknowledgments

This work was financially supported by the National Natural Science Foundation of China (No. 21675131) and the Municipal Science Foundation of Chongqing City (No. CSTC-2015jcyjB50001).

Notes and references

1 W. W. Zhao, J. J. Xu and H. Y. Chen, *Anal. Chem.* 2016, 82, 307-1 W. W. Zhao, J. J. Xu and H. Y. Chen, *Anal. Chem.* 2016, 82, 307-315.2
2. J. Shu and D. P. Tang, *Chem. Asian J.* 2017, 12, 2780-2789.
3 A. E. Becquerel, *C R Acad. Sci.* 1839, 9, 145-149.
4 X. Li, L. S. Zhu, Y. L. Zhou, H. S. Yin and S.Y. Ai, *Anal. Chem.* 2017, 89, 2369-2376.
5 S. J. Li, C. Y. Li, Y. F. Li, J. J. Fei, P. Wu, B. Yang, J. Ou Yang and S. X. Nie, *Anal. Chem.* 2017, 89, 6854-6860.
6 Q. Z. Han, R.Y. Wang, B. Xing, T. Zhang, M. S. Khan, D. Wu and Q. Wei, *Biosens. Bioelectron.* 2018, 99, 493-499.
7 X. P. Wang, R. Xu, X. Sun, Y. G. Wang, X. Ren, B. Du, D. Wu and Q. Wei, *Biosens. Bioelectron.* 2017, 96, 239-245.
8 C. Ye, M. Q. Wang, Z. F. Gao, Y. Zhang, J. L. Lei, H. Q. Luo and N. B. Li, *Anal. Chem.* 2016, 88, 11444-11449.
9. K. Y. Zhang, S. Z. Lv, Z. Z. Lin, M. J. Li and D. P. Tang, *Biosens. Bioelectron.* 2018, 101, 159-166.
10. Q. Z., Y. X. Lin, K. Y. Zhang, M. J. Li and D. P. Tang, *Biosens. Bioelectron.* 2018, 101, 146-152.
11 C. Ye, M. Q. Wang, L. J. Li, H. Q. Luo and N. B. Li, *Nanoscale* 2017, 9, 7526-7532.
12. K. Y. Zhang, S. Z. Lv, Z. Z. Lin and D. P. Tang, *Biosens. Bioelectron.* 2017, 95, 34-40.
13 D. J. Yang, H. W. Liu, Z. F. Zheng, Y. Yuan, J. C. Zhao, E. R. Waclawik, X. B. Ke and H. Y. Zhu, *J. Am. Chem. Soc.* 2009, 131, 17885-17893.
14 L. Zhang, D. W. Jing, X. L. She, H. W. Liu, D. J. Yang, Y. Lu, J. Li, Z. F. Zheng and L. J. Guo, *J. Mater. Chem. A.* 2014, 2, 2071-2078.
15 T. L. Thompson and J. T. Yates, *Chem. Rev.* 2006, 106, 4428-4453.
16 X. B. Chen and S. S. Mao, *Chem. Rev.* 2007, 107 (7), 2891-2959.
17 M. Anpo and M. Takeuchi, *Int. J. Photoenergy* 2001, 3, 89-94.
18 A. Paola Di, S. Ikeda, G. Marc`ı, B. Ohtani and L. Palmisano, *Int. J. Photoenergy* 2001, 3, 171-176.
19 C. C. Hu, T. C. Hsu and L. H. Kao, *Int. J. Photoenergy* 2012, 2012, 1-9.
20 T. C. An, J. X. Chen, G. Y. Li, X. J. Ding, G. Y. Sheng, J. M. Fu, B. X. Mai and K. E. O'Shea, *Catal. Today* 2008, 139, 69-76.
21 S. S. Zhao, S. Chen, H. T. Yu and X. Quan, *Sep. Purif Technol.* 2012, 99, 50-54.
22. J. Shu, Z. l. Qiu, S. Z. Lv, K. Y. Zhang, and D. P. Tang, *Anal. Chem.* 2018, 90, 2425-2429.
23 Q. Kang, X. X. Wang, X. L. Ma, L. Q. Kong, P. Zhang and D. Z. Shen, *Sens. Actuators, B.* 2016, 230, 231-241.
24 T. Ohno, M. Akiyoshi, T. Umebayashi, K. Asai, T. Mitsui and M. Matsumura, *Appl. Catal, A* 2004, 265, 115-121.
25 Y. V. Kolen'Ko, A. V. Garshev, B. R. Churagulov, S. Boujday, P. Portes and C. Colbeau-Justin, *J. Photochem. Photobiol. A* 2005, 172, 19-26.
26 R. Zhu, C. Y. Jiang, B. Liu and S. Ramakrishna, *Adv. Mater.* 2009, 21, 994-1000.
27 G. L. Wang, J. J. Xu, H. Y. Chen and S. Z. Fu, *Biosens. Bioelectron.* 2009, 25, 791-796.
28 W. W. Zhao, L. Zhang, J. J. Xu and H. Y. Chen, *Chem. Commun.* 2012, 48, 9456-9458.
29. Z. l. Qiu, J. Shu, and D. P. Tang, *Anal. Chem.* 2018, 90, 1021-1028.
30 N. M. Dimitrijevic, Z. V. Saponjic, B. M. Rabatic and T. J. Rajh, *Am. Chem. Soc.* 2005, 127, 1344-1345.
31 A. P. Xagas, M. C. Bernard, A. Hugot-Le Goff, N. Spyrellis, Z. Loizos and P. J. Falaras, *Photochem. Photobiol. A: Chem.* 2000, 132, 115-120.
32 T. Rajh, L. X. Chen, K. Lukas, T. Liu, M. C. Thurnauer and D. M. Tiede, *J. Phys. Chem. B* 2002, 106, 10543-10552.
33 E. L. Tae, S. H. Lee, J. K. Lee, S. S. Yoo, E. J. Kang and K. Yoon, *B. J. Phys. Chem. B* 2005, 109, 22513-22522.
34 W. Kubo and T. Tatsuma, *J. Am. Chem. Soc.* 2006, 128, 16034-16035.
35 C. G. Qian, S. Zhu, P. J. Feng, Y. L. Chen, J. C. Yu, X. Tang, Y. Liu and Q. D. Shen, *ACS Appl. Mater. Interfaces* 2015, 7, 18581-18589.
36 J. Zhuang, D. Tang, W. Lai, M. Xu and D. Tang, *Anal. Chem.* 2015, 87, 9473-9480.
37 W. W. Zhao, J. Wang, Y. C. Zhu, J. J. Xu and H. Y. Chen, *Anal. Chem.* 2015, 87, 9520-9531.
38. J. Li, M. Zhang, X. Li, Q, Y. Li and J. J. Yang. *Applied Catalysis B: Environmental* 2017, 212, 106-114.
39 Z. Tian, Q. Li, Y. Li and S. Ai, Catal. Commun. 2015, 61, 97-101.
40 X. J. Li, S. Q. Yu, T. Yan, Y. Zhang, B. Du, D. Wu and Q. Wei, *Biosens. Bioelectron.* 2017, 89, 1020-1025.
41 P. Niu, G. Liu and H. M. Cheng, *J. Phys. Chem. C* 2012, 116, 11013-11018.
42 Z. Sheng, L. Shao, J. Chen, W. Bao, F. Wang and X. Xia, *ACS Nano* 2011, 5, 4350-4358.
43 Q. Li, L. Zong, Y. Xing, X. Wang, L. Yu and J. Yang, Sci. *Adv. Mater.* 2013, 5, 1316-1322.
39 Y. Li, H. Zhang, P. Liu, D. Wang, Y. Li and H. Zhao, *Small* 2013, 9, 3336-3344.
45 P. Stefanov, M. Shipochka, P. Stefchev, Z. Raicheva, V. Lazarova and L. Spassov, J. Phys.: Conf. Ser., 2008, 100, 012039.
46 G. Van der Laan, C. Westra C. Haas and G. A. Sawatzky, *Phys. Rev.* 1981, 23, 4369.
47 Q. B. Li, X. Zhao, J. Yang, C. J. Jia, Z. Jin and W. L. Fan, *Nanoscale* 2015, 7, 18971-18983.
48 K. Gibson, J. Glaser, E. Milke, M. Marzini, S. Tragl, M. Binnewies, H. A. Mayer and H. JürgenMeyer, *Materials Chemistry and Physics* 2008, 112, 52-56.
49 L. Liu, D. Ma, H. Zheng, X. J. Li, M. J. Cheng and X. H. Bao, *Mesoporous Mater.* 2008.110, 216-222.
50 H. J. Yan and H. X. Yang, *Journal of Alloys and Compounds* 2011, 509, 26-29.
51 X. C. Wang, K. Maeda, A. Thomas, K. Takanabe, G. Xin, J. M. Carlsson, K. Domen and M. Antonietti, *Nat. Mater.* 2008, 8, 76-80.
52 D. W. Fan, C. J. Guo, H. M. Ma, D. Zhao, Y. N. Li, D. Wu and Q. Wei, *Biosens. Bioelectron.* 2016, 75, 116-122.
53 G. L. Wang, J. J. Xu, H. Y. Chen and S. Z. Fu, *Biosens.Bioelectron.* 2009a, 25, 791-796.
54 D. J. Yang, J. Zhao, H. W. Liu, Z. F. Zheng, M. O. Adebajo, H. X. Wang, X. T. Liu, H. J. Zhang, J. C. Zhao, J. Bell and H. Y. Zhu, *Chem.-Eur. J.* 2013, 19, 5113-5119.
55 T. Rajh, N. M. Dimitrijevic, M. Bissonnette, T. Koritarov and V. Konda, *Chem. Rev.* 2014, 114, 10177-10216.
56. G. C. Fan, H. Zhu, Q. M. Shen, L. Han, M. Zhao,J. R. Zhang and J. J. Zhu, *Chem. Commun.* 2015, 51, 7023-7026.
57. G. C. Fan, H. Zhu, D. Du, J. R. Zhang, J. J. Zhu, and Y. H. Lin, *Anal. Chem.* 2016, 88, 3392−3399.
58 M. T. Mazorra, J. A. Rubio and J. Blasco, *Comp. Biochem. Physiol. B,* 2002, 131, 241-249.
59 F. M. Hagit, and A. David, *J. Am. Chem. Soc.* 2005, 127, 8077-8081.
60 X. Li, Y. Zhou, Y. Xu, H. Xu, M. Wang, H. Yin and S. Ai, *Anal. Chim. Acta* 2016, 934, 36-43.
61 J. J. Deng, P. Yu, Y. X. Wang and L. Q. Mao, Anal. Chem. 2015, 87, 3080-3086.

View Article Online
DOI: 10.1039/C8AN00895G

Analyst

ARTICLE

View Article Online
DOI: 10.1039/C8AN00895G

Table of contents

A novel "signal-on" photoelectrochemical sensing for ultrasensitive detection of alkaline phosphatase activity based on TiO_2/g-C_3N_4 heterojunction

Feng Xia Wang, Cui Ye, Shi Mo, Liu Li Liao, Xiao Fang Zhang, Yu Ling, Lu Lu, Hong Qun Luo* and Nian Bing Li*

A novel "signal-on" photoelectrochemical sensing for ultrasensitive detection of alkaline phosphatase activity was developed using TiO_2/g-C_3N_4 heterojunction.